Climatological patterns over South America derived from COSMIC radio occultation data

R. Hierro,[1] P. Llamedo,[1] A. de la Torre,[1] P. Alexander,[2] and A. Rolla[1]

rhierro@austral.edu.ar

[1]Facultad de Ingeniería, Universidad Austral, Avda. Garay 125, 5to Piso, C1063ABB Buenos Aires, Argentina

[2]Departamento de Física, Facultad de Ciencias Exactas y Naturales, Universidad de Buenos Aires, Ciudad Universitaria, 1428 Buenos Aires, Argentina

Abstract.

Meteorological phenomena are closely linked to the presence of water vapor. They are mainly originated and developed in the troposphere, where almost all the atmospheric water is concentrated. The Global Positioning System Radio Occultation (GPS RO) technique provides vertical profiles of atmospheric properties such as refractivity, from which temperature and water vapor are derived. The GPS RO capability to reproduce global, aynoptic and regional climatological patterns over South America, which is a mostly oceanic continent, is tested. From FORMOSAT-3/COSMIC mission data (2006-2010), our previous knowledge regarding global and synoptic/regional patterns of temperature, equivalent potential temperature, specific humidity and pressure is verified. Special cases such as baroclinic disturbances arriving at South America midlatitudes and storm events over a mountain region near the Andes are analyzed. The temporal evolution and the latitude-longitude distribution in several layers of the variables listed above are well described with this technique. Water vapor is one of the most important variables in the troposphere because of its influence in the energy transport and circulation within the Earth weather and climate system through latent heat exchange. Besides, it is the most important greenhouse gas in the atmosphere. Water vapor largely affects the radiative balance of the Earth surface and the extent and type of the continental biosphere.

1. Introduction

For decades the radiosonde network has provided all-weather in situ water vapor measurements but in a very limited and inhomogeneous area. Nowadays, satellite instruments provide high resolution humidity profiles with a global coverage. In particular, The Global Positioning System (GPS) Radio Occultation (RO) technique is a powerful tool to study the global distribution of water vapor with a moderate/high spatial and temporal resolution. The GPS RO technique provides vertical profiles of atmospheric properties such as refractivity, from which density, pressure, temperature and water vapor pressure are derived. The Constellation Observing System for Meteorology Ionosphere and Climate/Formosa Satellite 3 (shortened as COSMIC hereafter) mission provides about 1800 daily RO profiles with an almost uniform global coverage. The vertical resolution of RO profiles range from 0.2 km in the lower troposphere to 1.4 km in the stratosphere [*Kursinski et al,* 1997]. However, COSMIC post processed profiles are available from near the surface to up to 40 km, interpolated every 0.1 km. The "open-loop" mode tracking routine [*Anthes et al,* 2008] used in COSMIC retrievals significantly reduces the inversion biases by eliminating tracking errors [*Sokolovski et al,* 2007], extending those retrievals down to the Earth's surface. This is very important for the study of water vapor variation and its distribution in the lower troposphere.

Ho et al (2010) compared the specific humidity profiles derived from COSMIC with those of global ECMWF analysis over different regions, during both day time and night time, and found an almost zero mean bias. *Kishore et al* [2011] studied the distribution of water vapor between 50S and 50N observed by COSMIC and compared it with GPS radiosonde

data sets. A good agreement was found, up to 8 km, suggesting that COSMIC water vapor data are reliable in the troposphere. This demonstrates the high quality of COSMIC water vapor profiles in the middle and lower troposphere, and shows their usefulness as an independent reference for quantifying humidity uncertainties among different sensors.

This work is motivated by the insufficient measurement over South America. The aim is to evaluate the capability of GPS-RO to represent tropospheric processes throughout different meteorological fields. The latter are widely associated to water vapor, which is mostly concentrated at low-level of the troposphere. In section 2, regional features of South America are introduced. In section 3 COSMIC RO data (2006-2010) description and the methodology employed are presented. In section 4, the global distribution of low-level specific humidity is examined and time evolutions over selected areas as well as the synoptic/regional fields over South America are presented and discussed.

2. Regional characteristics

South America is characterized by its large-covering oceanic area and its unique topography, which consists in a North-South barrier with tops up to 7 km, from the Equator to 55S, blocking the zonal flow over the Southern Hemisphere and impacting the regional circulation by determining the position of the planetary waves [*Seluchi et al,* 2003]. According to *Zhou and Lau* [1998], the South American Monsoon System (SAMS) starts its development during spring over South America. This is featured by a southward shift in convection, dominant over the highland region of the Central Andes and Amazonia and merging with the South Atlantic Convergence Zone (SACZ), while the Intertropical Convergence Zone (ITCZ) in the eastern Pacific and western Atlantic, weakens. As it was stated by *Vera et al* (2006), SAMS exhibit a surface low pressure and an upper level

anticyclone with seasonal changes in precipitation (increases and decreases) associated to an intense low-level inflow of moisture into the continent. This is under the dynamical influence of the Andes, which favors a poleward flow east of them all the year [*Nogues-Paegle et al,* 1998]. The regional circulation over the south of South America has been studied by several authors: the summer continental heating gives rise to the formation of a quasi-permanent low pressure system over the Chaco region (between Paraguay and Bolivia) which extends meridionally on the lee side of the Andes, from the Amazon to northwestern Argentina [*Seluchi et al,* 2003]. On the other hand, *García-Ortega et al* (2009) marked that this part of the continent shows a high frequency of severe convective storms with intense precipitation, large hailstones, damaging winds and occasional tornados. They pointed out that in this setting, the combination of subsynoptic factors such as diurnal warming, convective instability, or moisture flux convergence, may trigger mesoscale convection. Several authors have noted a maximum in the low-level moisture about 30S-40S during the austral summer, associating this enhancement with the deep convection in the region [*de la Torre et al, 2004; Simonelli et al, 2006; Teitelbaum et al, 2008*]. *Velasco and Fritsch* (1987) surveyed the mesoscale convective complexes (MCCs) over South America using Geostationary Operational Environmental Satellite (GOES) infrared imagery, and found a large population of them over the east of the continent between 20- 40S, specially during December and January. Those MCCs tend to develop during the evening and reach their maximum size after midnight. In this respect, two useful variables to evaluate this situation are: specific humidity (q) and the equivalent potential temperature (θ_e). While the former gives information about the water vapor, the latter constitutes a good measure of heat and moist air content in an air parcel.

3. Data set and methodology

COSMIC post-processed level 2 "wet" data provide temperature (T), pressure (P) and water vapor pressure (e) vertical profiles from near the surface up to 40 km, interpolated every 0.1 km. COSMIC data are binned into longitude, latitude, altitude and time grid cells and then averaged using different grid cell sizes, according to the process shown below.

From COSMIC data, the specific humidity (q) is calculated as:

$$q = \frac{w}{1+w} \tag{1}$$

where $w = 0.622\frac{e}{P-e}$ is the water vapor mixing ratio. Then, the equivalent potential temperature (θ_e) is calculated as:

$$\theta_e \approx \left(T + \frac{L_v}{c_p} w\right)\left(\frac{P_0}{P}\right)^{\frac{R_d}{c_p}} \tag{2}$$

where R_d is the specific gas constant for air, L_v is the latent heat of evaporation and c_p is the specific heat of dry air at constant pressure. By definition, θ_e allows differentiating two air masses, warm-wet and cold-dry, respectively. It is useful to recognize baroclinic zones, where a strong contrast in θ_e may indicate the presence of a cold/warm front. Hereinafter, the variables will be denoted as "low-level" (subindex LL) when they are averaged between two selected heights below 3 km. For example, for q averaged between z_1=2 km and z_2=3, it will be denoted as q_{LL} (low-level specific humidity).

4. Results

4.1. Specific humidity global fields

Figure 1 shows the averaged fields of precipitable water (PW) defined by $PW = \frac{1}{g}\int_{P_1}^{P_2} w.dp$, for austral winter (JJA) and summer (DJF) using NCEP FNL (National Cen-

ters for Environmental Prediction-(Final) global gridded analysis archive) with 1° horizontal resolution and 27 verticals vertical levels. Different monsoon systems are observed in both seasons, such as the North American Monsoon System, the African Monsoon System, the Indian Monsoon System, the East Asia Monsoon System and the South East Asia Monsoon System for JJA and South America Monsoon System (SAMS) and the Australian Monsoon System for DJF. COSMIC data are averaged seasonally and in height (0-3 km) inside every 1°x1° latitude longitude grid cell (Figures 1 c and d). A high correlation between high PW and q_{LL} values may be observed. It is possible to distinguish every region including a monsoon system only from q_{LL}. In particular, taking into account that during DJF the SAMS reaches its mature phase [Vera et al, 2006], the seasonal evolution of q_{LL} over region (6) (5-15S, 50-65W) is shown in Figure 2. Here, a monthly average is applied to smooth the signal. From the period June 2006-June 2010, the decreasing/increasing q_{LL} values during JJA/DJF, are clear.

4.2. Synoptic scale fields

The P_{LL} fields for DJF and JJA are shown in Figures 3a and b. The climatological positions of the Pacific and Atlantic semi-permanent anticyclonic systems are evident during both seasons [*Garreaud and Wallace* 1997]. As expected, the two systems are intensified during DJF, acompanied by a southward displacement. The inferred low-level circulation from Figures 3a and b is analogous to that described by other authors [i.e. *Campetella and Vera*, 2002] and it is illustrated by Figure 4. Here, a northerly flow is produced by the counterclockwise circulation associated to the South Atlantic anticyclone and a relative low pressure system developed over the center/south of the continent, known as Chaco Low (CHL) [*Seluchi et al,* 2003]. It is a thermal system

and therefore it weakens with increasing height and reverses in upper-level [*Seluchi et al,* 2003 and references therein]. Even though it is present in the annual mean field, it is intensified during DJF [*Seluchi et al,* 2000]. Figures 3c and d show mid-level pressure fields (smoothed and averaged in 5-6 km), for both seasons. In accordance with the described above, Figure 3d indicates that during DJF a long wave trough over the CHL is present at mid-level, while at upper-level, it reverses to form a ridge (see dotted lines in Figures 3d and 3f). Other aspects observed at upper-level are: i) the northward JJA displacement of the systems at midlatitudes, ii) the high pressure system known as Bolivian High (BH) centered about 10S, which is the dominant South America upper-level circulation feature and iii) the presence of a strong ridge to the east, between 20-40W, known as the Northeast High. Both ii) and iii) are well described in *Lenters and Cook* [1997].

In Figures 5a and b $\theta_{e(LL)}$ for both seasons is shown. During JJA (Figure 5a), low values of $\theta_{e(LL)}$ are located from the central to the southern part of the domain. A barotropic stratification over the whole region is evident, even over the continental zone. During DJF (Figure 5b) a zonal maximum at midlatitudes is observed over the continent, yielding to the presence of a warm and wet "tongue" over the North/Center of Argentina. The synoptic scale q_{LL} for both seasons is presented in Figures 5c and d. During JJA, lower values are observed over the whole Continent, (Figure 5c), with a maximum region over the Equator, extending towards central South America. During DJF (Figure 5d), higher values are present over the whole continent and the area containing the maximum is located South of the Equator, over the Amazonas and decreasing towards the north of Argentina. At midlatitudes, a relative maximum over the continent is present, probably associated to a warm and wet air transport from lower to higher latitudes, whose associated

inflow was described by *Seluchi and Marengo* (2000) and *Garreaud* (2009). From q_{LL}, the presence of both the Pacific and Atlantic anticyclones is more evident during DJF, with low values over the eastern branches of the two systems (see detail "d" in figure 3), which are typically dry zones in maritime tropical air masses [*Pettersen*, 1941]. These JJA and DJF patterns match with those described in several studies for other variables, such as outgoing longwave radiation, precipitation or cloud distribution over South America [i.e. *Marengo et al,* 2004, *Vera et al,* 2006]. The vertical structures of specific humidity are analyzed in Figures 5e and f, showing Z-lat (60-65W) slices for both seasons. The presence of a low-level moist core centered over the Equator is clear during JJA (Figure 5e), showing high values up to 15S, and decreasing towards the South. During DJF (Figure 5f), an increase of this variable is observed between 15-35S and the moist core is displaced towards the pole, centering about 15-20S. At those latitudes, it is possible to localize its major vertical extension, reaching altitudes of 8-9km, with values $\approx 3.10^{-4} g/kg$

4.3. Time evolution

The q_{LL} seasonal feature observed over Argentina (25-55S)-(70-55W) in Figures 3c and d, as well as the low-level circulation associated to P_{LL}, were evaluated from the time evolution analysis of both variables. The methodology employed is as follows:

i) Two regions were selected: one located over Argentina with coordinates (20-35S)-(55-69W), (hereinafter "LP"), which covers the influence zone of the Low Pressure system represented in Figure 4, and another over the Atlantic ocean, covering the Atlantic Anticyclone influence zone (hereinafter "AA"), with coordinates (20-40S)-(10-30W); ii) the time evolution of q_{LL} and P_{LL} in LP and AA were obtained and then a smoothing average

was applied to each one; iii) to make the comparison between them possible, the resultant signals were then standardized, making

$$P_* = \frac{P_{LL} - \overline{P_{LL}}}{\sigma_P}, q_* = \frac{q_{LL} - \overline{q_{LL}}}{\sigma_q} \quad (3)$$

where $\overline{P_{LL}}$, $\overline{q_{LL}}$, σ_P, σ_q are the corresponding mean value and standard deviation for each variable. The joint evolutions of P_* and q_* over LP and over AA were analyzed. These results are presented in Figure 6. q_*^{LP} (Figure 6a) shows the same behaviour observed in Figure 2 for q_{LL} over SAMS region, with low values during JJA and high values during DJF. As it was stated above, during DJF a low pressure system (Chaco Low) deepens over Argentina. At this time, P_*^{LP} (Figure 6b) shows decreasing values, while q_*^{LP} increases. During DJF, there is a 180° phase shift between both signals, being q_*^{LP} maximum while P_*^{LP} is mimimum. In December 2009, this indirect behavior is observed, although not so marked. Figure 6c shows the time evolutions of P_*^{AA} and q_*^{LP}. For the 2006, 2007 and 2008 signals it is possible to observe a joint increase of the variables, mostly during DJF. Although such increase is not so clear during DJF 2009, there is a P_*^{AA} minimum in December and after this, a slight increase, again in phase with q_*^{LP}. This is in agreement with the northern transport associated circulation described above (i.e. Figure 4) and with the results obtained from Figure 6b. All these features confirm the good agreement between the RO pressure fields and the known northern transport and low-level circulation over South America, as well as the capability of the technique to provide a good spatial synoptic variability of P and q, and their associated variables.

4.4. Regional fields

The South of South America is a baroclinic zone, where the front passages are abundant during all the year and in particular during JJA. The central part of Argentina (south of 25S) was selected to evaluate the capability to reproduce smaller scale meteorological phenomena: We considered: i) 40 cold front events during JJA over the region to be compared with the JJA period averaged and ii) 43 events of severe hailstorms occurred in Mendoza, (Argentina) roughly located between (32-36S)-(65-69W) during 2006-2010 to be compared with the whole period averaged, respectively. Here, we take into account that it is possible to assume a normal distribution in the two cases. Figures 7a and b depict $\theta_{e(LL)}$ for the JJA period and for the 40 cold front cases averaged, respectively. The dark zone indicates the transition zone between two air masses and, as expected, it is clearly marked in the frontal cases (Figure 7b) due to the stronger temperature contrast. Moreover, the baroclinic case is evident from the temperature field, showing the typical sinusoidal enhancement (along the dark region), and deviating the average $\theta_{e(LL)}$ from its JJA climatological zonal distribution (Figure 7a). Z-lat (55-60W) for JJA and for the front cases, are presented in Figures 7 c) and d), respectively. It is possible to observe clear differences between the two samples: a stronger temperature contrast in the front cases (figure 7d), depicted for the thinner contour separation, is evident from 35S to higher latitudes. Towards the South, the presence of colder air is marked from the lower values of $\theta_{e(LL)}$ (white zone). In the JJA period, the temperature distribution presents a not so clear cold core at high latitudes and the meridional contrasts are not so marked (weaker contour separations). Figure 7e compares the $\theta_{e(LL)}$ signal, smoothed for both samples at different latitudes (27-33S) as a function of longitude. The front cases present

the largest wave amplitude in all the domain for every latitude, probably associated to their typical sinusoidal temperature distribution, which yields to a differentiation with the more barotropic JJA case. The position of the baroclinic zone shown in Figure 7b is more evident from this figure, where a NW-SE horizontal tilting maximum is observed from the peaks. This seems to slow down to the West between 29-31S, showing a break in the signal and locating the strong baroclinicity between 40-60W.

Figures 8a and b present q_{LL} for (2006-2010) period and storms events (SE) average, respectively. In the SE case (figure 8 b) higher values of q_{LL}, when compared to those observed in the 2006-2010 frame (figure 7 a) are present over the North and the central zone of the domain. $\theta_{e(LL)}$ presents a positive anomalous area over the study region (not shown) indicating that, as expected in the case of SE, the GPS-RO data revealed a region dominated by a warmer and wetter air mass than the average. In Figures 8c and d we calculated the anomalies from $\widetilde{q}_{LL}$= q_{LL}(SE) - q_{LL}(2006-2010). It makes $\widetilde{q}_{LL} > 0$ (< 0) when q_{LL}(SE) is higher (lower) than q_{LL} 2006-2010 period. The features mentioned above can be confirmed from Figures 8c and d, which show $\widetilde{q}_{LL}$ Z-lat (60-65W) and Z-lon (30-40S) slices (red line in Figures 8a and b). From Figure 8d it is possible to observe, in general, positive values of $\widetilde{q}_{LL}$ at all latitudes and in particular, over the studied region at the south of 30S, with two relative maximums near 34-37S. In the Z-lon slice (Figure 8d) higher values of $\widetilde{q}_{LL}$ are present at the east of the Andes over the region of interest, with a maximum close to 65W. Clearly, the technique is indicating an increase of water vapor content in the storm events over Mendoza.

5. Conclusions

At a global scale from GPS RO data, it is possible to distinguish the Monsoon Systems which have been studied up to now, for selected JJA and DJF averages in both hemispheres. q_{LL} shows a coherent evolution over the South American Monsoon System, with low values during JJA and high values during DJF.

Over South America :

• At low-level, the South Atlantic and South Pacific anticyclones are well represented, such as the thermal system known as Chaco Low around 25S, which intensifies during summer. At mid-levels, a long-wave trough associated to the above mentioned system is clearly distinguishable. At upper-level, a high pressure DJF pattern known as Bolivian High is centered at about 15S, while to the South, it is possible to observe a strong ridge, probably associated with the inversion which occurs above to the Chaco Low.

• The seasonal $\theta_{e(LL)}$ shows high values, incoming from the Amazonas towards higher latitudes during DJF. It penetrates the North of Argentina, giving rise to the presence of a warm and wet tongue over this region. This $\theta_{e(LL)}$ distribution coincides with the inferred circulation from the P_{LL} fields above described, which in turn show the same features described by other authors, in relation to the seasonal circulation over the continent. Similar features for q_{LL} are observed: Z-lat slices for both seasons confirm the presence of a moist core in 60-65W centered at low latitudes during JJA and extending towards the South covering midlatitudes during DJF.

• The P_{LL} time evolution analysis at low-level over selected areas states a correlation between them, which coincides in the maximum with i) the DJF northern circulation

found in P_{LL} and in the ii) $\theta_{e(LL)}$ fields here detected and already described by other authors.

• For 40 selected JJA front cases arriving at midlatitudes, $\theta_{e(LL)}$ derived from this technique exhibited an expected behaviour, showing a withdrawal from the more barotropic case obtained for JJA case. The baroclinic zone is clearly distinguishable at low-level as well as in Z-lat slices between 55-60W, where it is possible observe strong contrasts of $\theta_{e(LL)}$ which makes it possible to locate the front position and its vertical structure.

• 43 cases of hail storm events (SE) were selected over a mountain region near the Andes, between 32-36S and 65-69W, in order to analyze a smaller scale performance of the technique. A comparison of q_{LL} between in SE cases and the averages for the 2006-2010 period, reveals that the expected increase in $\theta_{e(LL)}$ is present in SE over the studied region, while high values of q_{LL} are incoming from the North. Z-lat and Z-lon anomalies slices show several peaks, which coincide in both cases with the area of SE occurrence.

GPS RO data demonstrates to be an useful tool able to construct meteorological fields in the lower and middle troposphere, on global, synoptic and regional (South America) scale.

Acknowledgments. (Text here)

References

Anthes, R. A., and oauthors, 2008: The cosmic/formosat-3 mission: early results. Bull. Amer. Meteor. Soc., 89, 313-333. doi: 10.1175/BAMS-89-3-313.

Campetella, C. and C. Vera, 2002: The influence of the Andes mountains on the South America low-level flow. Geophys. Res. Lett., 29, (17), 1826, doi:10.1029/2002GL015451

de la Torre, A., D. Vincent, R. Tailleaux, H. Teitelbaum, 2004: A deep convection event above the Tunuyn Valley near to the Andes Mountains. Mon. Weather Rev. 132 (9), 2259-2268.

García-Ortega, E., L. Lpez and J. L. Snchez, 2009: Diagnosis and sensitivity study of two severe storm events in the Southeastern Andes. Atmos. Res. 93, 161-178.

Garreaud, R. D. and J. M. Wallace, 1997: The diurnal march of the convective cloudiness over the Americas. Mon. Wea. Rev., 125, (12) 3157-3171

Garreaud, R., 2009: The Andes climate and weather. Adv. Geosciences, 7, 1-9.

Ho S.-P., X. Zhou, Y.-H. Kuo, D. Hunt and J.-H. Wang, 2010: Global Evaluation of Radiosonde Water Vapor Systematic Biases using GPS Radio Occultation from COSMIC and ECMWF Analysis. Remote Sens., 2, 1320-1330; doi:10.3390/rs2051320.

Houze, R. A., Jr., 1993: Cloud Dynamics. Academic Press, San Diego, 573 pp.

Kuo, Y.-H., T.-K. Wee, S. Sokolovskiy, C. Rocken, W. Schreiner, D. Hunt, and R. A. Anthes, 2004: Inversion and error estimation of GPS radio occultation data. J. Meteor. Soc. Japan, (82), 507-531.

Shu-peng Ho, Xinjia Zhou, Ying-Hwa Kuo, Douglas Hunt, and Jun-hong Wang, 2010: Global Evaluation of Radiosonde Water Vapor Systematic Biases using GPS Radio Occultation from COSMIC and ECMWF Analysis. Remote Sens. 2, 1320-1330; doi:10.3390/rs2051320

P. Kishore, M. Venkat Ratnam, S.P. Namboothiri, Isabella Velicogna, Ghouse Basha, J.H. Jiang, K. Igarashi, S.V.B. Rao and V. Sivakumar, 2011: Global (50S50N) distribution of water vapor observed by COSMIC GPS RO: Comparison with GPS radiosonde, NCEP, ERA-Interim, and JRA-25 reanalysis data sets. J Atmos Sol Terr Phys (in

297 press), doi:10.1016/j.jastp.2011.04.017

298 Kursinski, E. R. et al. (1997), Observing Earth's atmosphere with radio occultation mea-
299 surement using the Global Positioning System. J. Geophys. Res., 102, 429-465.

300 Lenters J. D. and K. H. Cook, 1997: On the Origin of the Bolivian High and Related
301 Circulation Features of the South American Climate. J. Atmos. Sci., 54, 656-678

302 Marengo, J., W. Soares, C. Saulo and M. Nicolini, 2004: Climatology of Low-Level Jet
303 east of the Andes as derived from the NCEP-NCAR reanalyses. J. of Climate, 17, (12),
304 2261-2280.

305 Nogus-Paegle J., K. Mo, and J. Paegle, 1998: Predictability of the NCEP/NCAR reanal-
306 ysis model during austral DJF. Mon. Wea. Rev., 126, 3135-3152.

307 Petterssen, S., 1941: Introduction to Meteorology. McGraw - Hill Book Co., New York,
308 EUA, 236 pp.

309 Seluchi, M. E. and J. A. Marengo, 2000: Tropical-midlatitude ex-change of air masses
310 during DJF and JJA in SouthAmerica: Climatic aspects and examples of intense events.
311 Int. J. Climatol., 20, 1167-1190

312 Seluchi, M., A.C. Saulo, M. Nicolini and P. Satyamurty, 2003: The Northwestern Argen-
313 tinean Low: A Study of TwoTypical Events. Mon. Wea. Rev., 131, 2361-2378.

314 Simonelli S., F. Norte, N. Heredia and M. Seluchi, 2006: The storm of January 1, 2000,
315 north of the city of Mendoza. Atmsfera 20 (I) 1-23.

316 Sokolovskiy, S. V., C. Rocken, D. H. Lenschow, Y.-H. Kuo, R. A. Anthes, W. S. Schreiner
317 and D. C. Hunt. Observing the moist troposphere with radio occultation signals from
318 COSMIC. Geophys. Res. Lett., 34, L18802, doi:10.1029/2007GL030458

Teitelbaum, H., H. Le Treut, M. Moustaoui, G. C. Cabrera and G. Ibaez, 2008: Deep convection east of the Andes Cordillera: A test case analysis of airmas origin. Mon. Wea. Rev., 136, 2201- 2209.

Velasco, I. and J. M. Fritsch, 1987: Mesoscale Convective Complexes in the Americas. J. Geophys. Res., 92, 9591 - 9613.

Vera, C., Higgins, W., Amador, J., Ambrizzi, T., Garreaud, R., Gochis, D., Gutzler, D., Lettenmaier, D., Marengo, J., Mechoso, C.R., Nogues-Paegle, J., Silva Diaz, P.L. and C. Zhang, 2006: Towards a unified view of the American Monsoon System. J. Clim. 19, 4977-5000.

Whiteman, C. D., 2000: Mountain Meteorology: Fundamentals and Applications. Oxford University Press, New York, 355pp.

Zhou J, Lau K-M. 1998. Does a monsoon climate exist over South America? J. Clim. 11, 1020-1040.

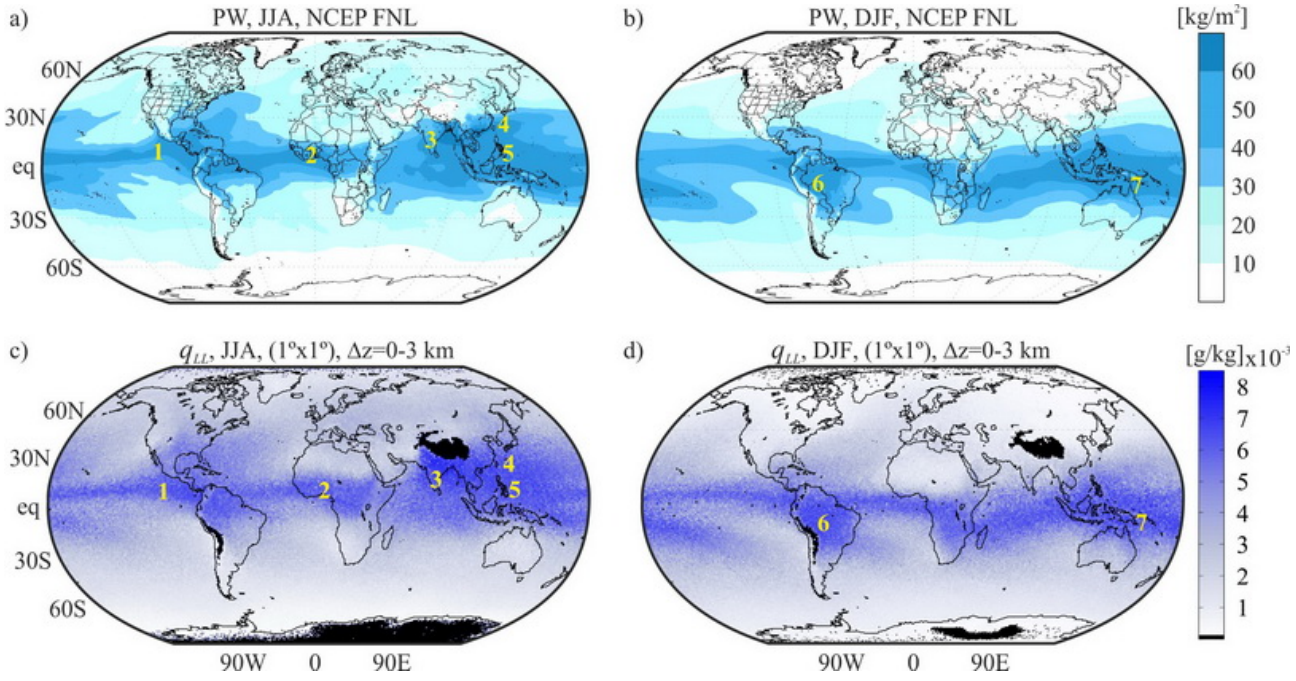

Figure 1. Averaged fields of PW from GFS-FNL for a) JJA and b) DJF respectively (see text). $(0-3)$ km averaged q with 1°x1° horizontal resolution for c) JJA and d) DJF.

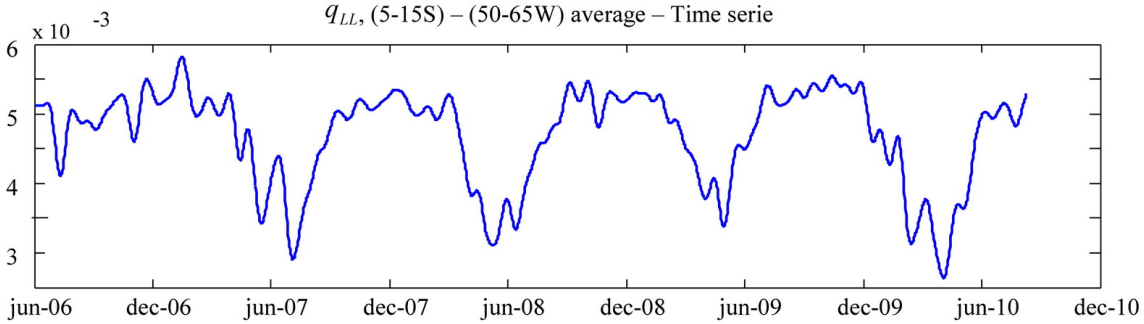

Figure 2. Time evolution of q_{LL} (smoothed) over SAMS region for the 2006-2010 period.

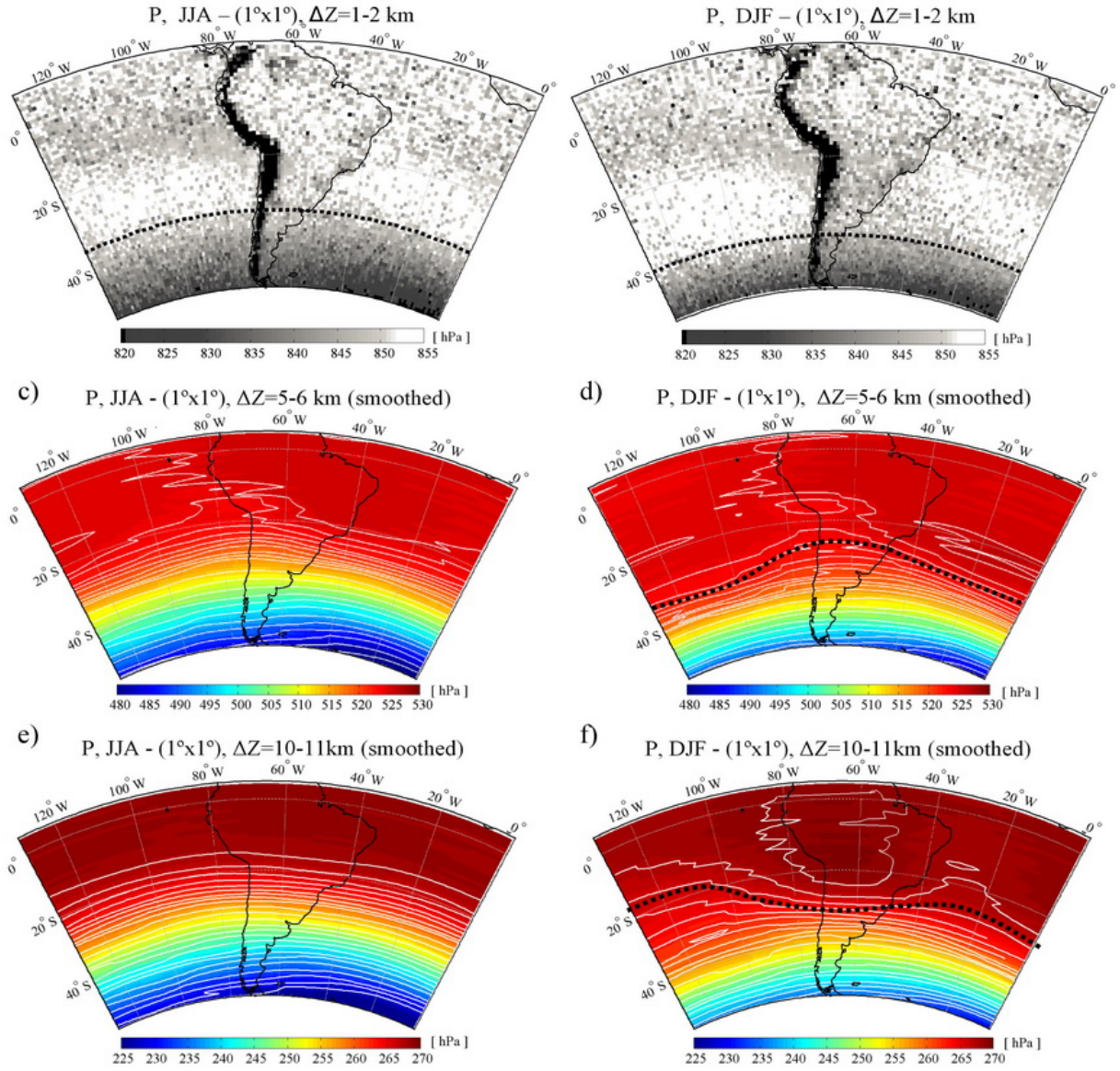

Figure 3. P_{LL} from COSMIC data, with 1°x1° horizontal resolution, for a) JJA and b) DJF. Dotted line indicate the transition between high and low pressure according to the scale employed; c) JJA and d) DJF mid-levels pressure (smoothed); e) JJA and f) DJF upper-levels pressure (smoothed). Dotted lines indicate the mid-level trough and upper level ridge.

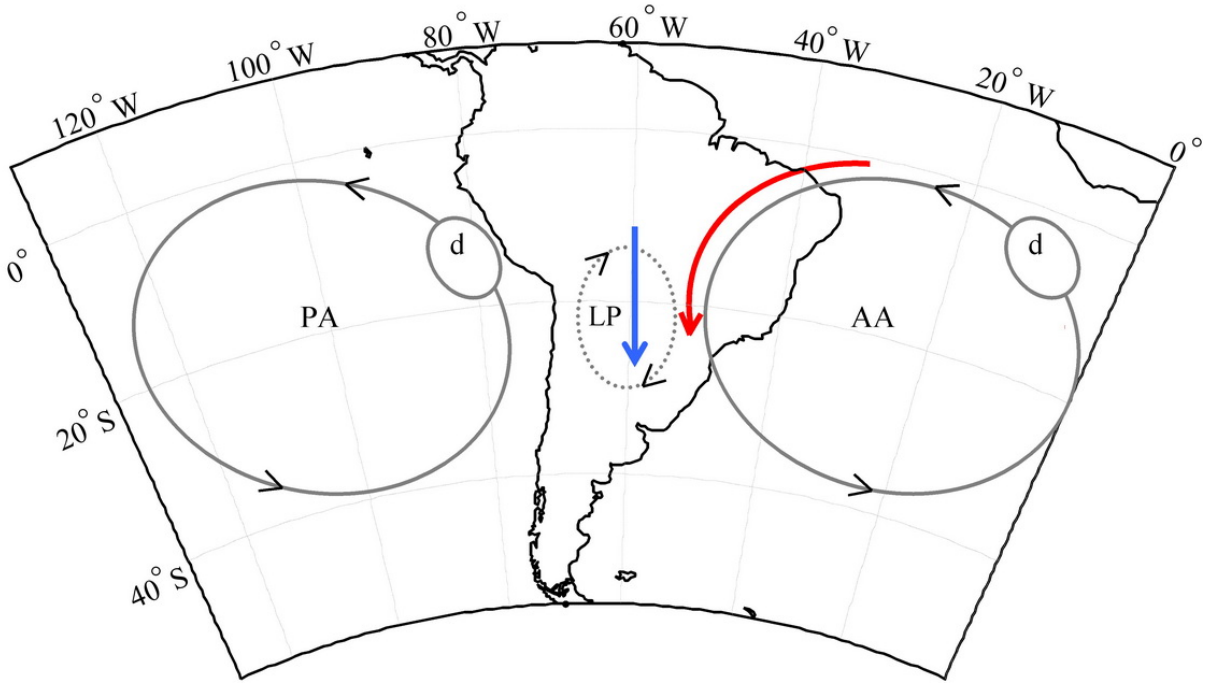

Figure 4. Schematic representation of the low-level circulation during DJF. AA: Atlantic Anticyclone, PA: Pacific Anticyclone, LP: Low Pressure System (Chaco Low). Dry zones are marked with "d".

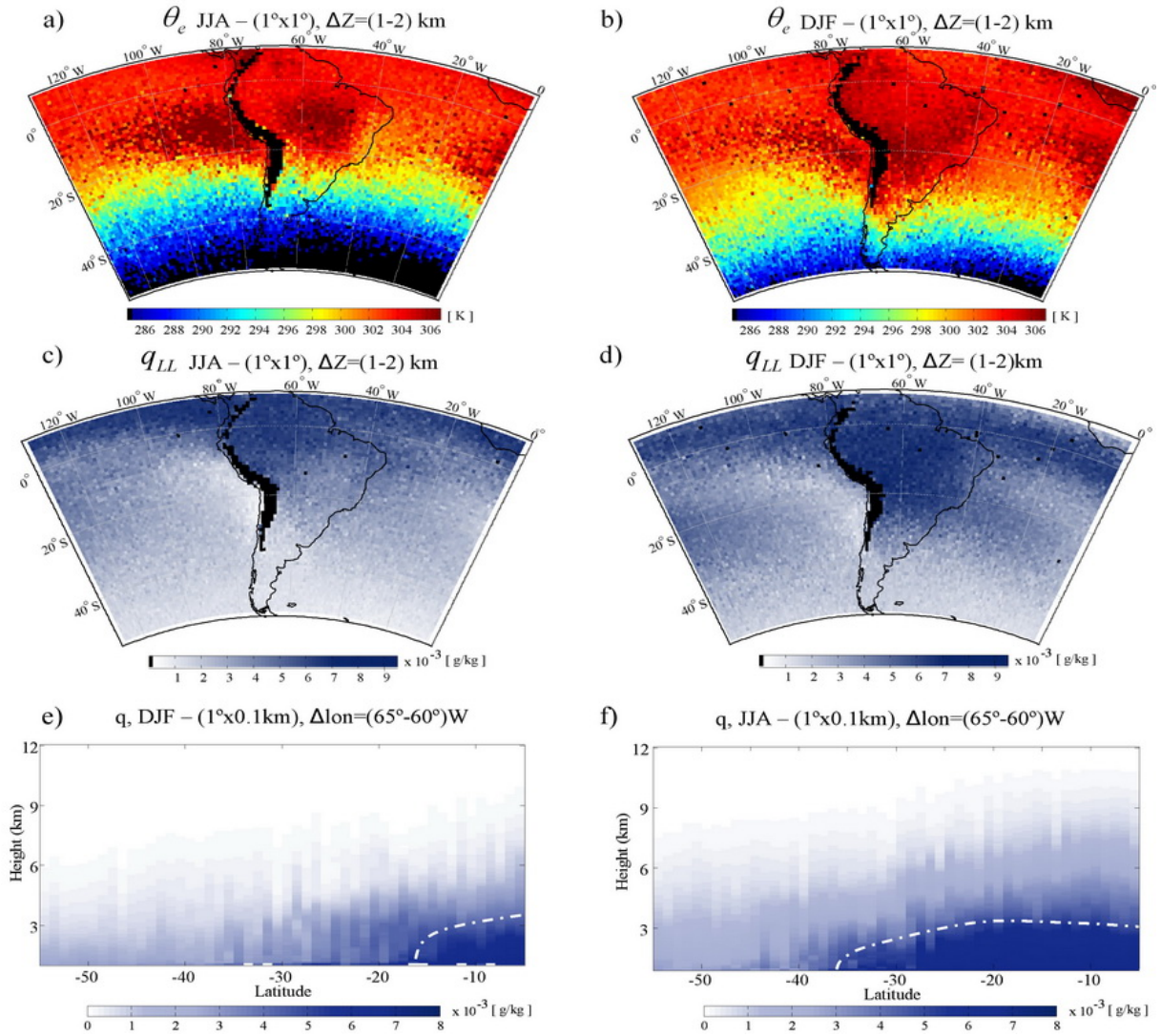

Figure 5. $\theta_{e(LL)}$ over South America for a) JJA and b) DJF; q_{LL} corresponding to c) JJA and d) DJF; q Z-lat slices for e) JJA and f) DJF, from 0 to 12 km. Dotted line marks a moist core over South America in both seasons.

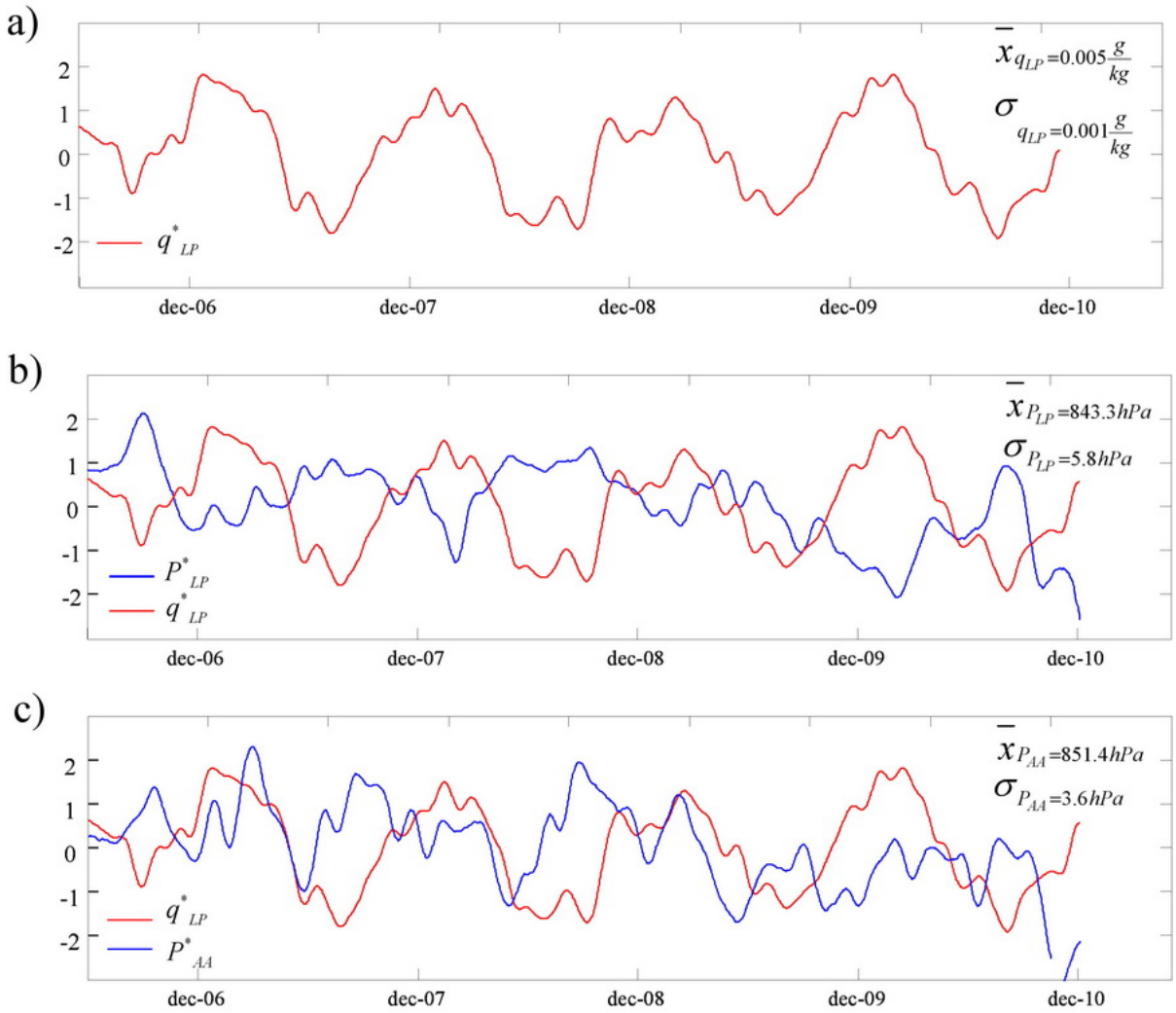

Figure 6. 2006-2010 time evolutions smoothed and standardized of a) q_*^{LP} over the LP region, (q_*^{LP}); b) idem a) for q_*^{LP} and P_{LL} (P_*^{LP}); c) q_*^{LP} and P_{LL} over the AA region (P_*^{AA}).

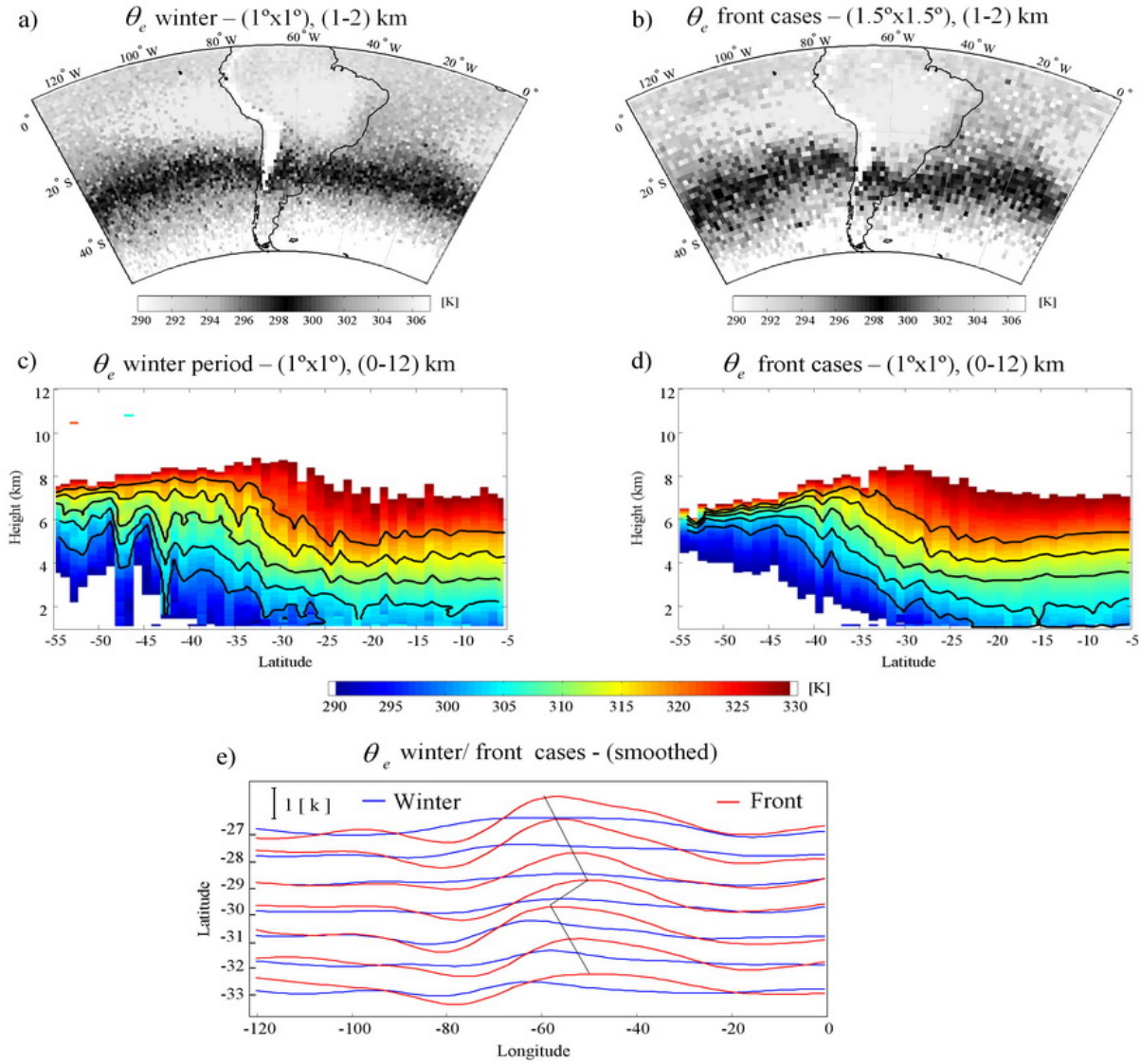

Figure 7. $\theta_{e(LL)}$ for a) JJA season and b) the cold front cases during JJA. The strong contrast in $\theta_{e(LL)}$ is dark shaded; c) and d) $\theta_{e(LL)}$ Z-lat slices for cases a) and b); e) smoothed $\theta_{e(LL)}$ for JJA season (blue) and JJA cold fronts (red), from 120W to 0W and different latitudes, from 27S to 33S. The dark line indicates the maxima.

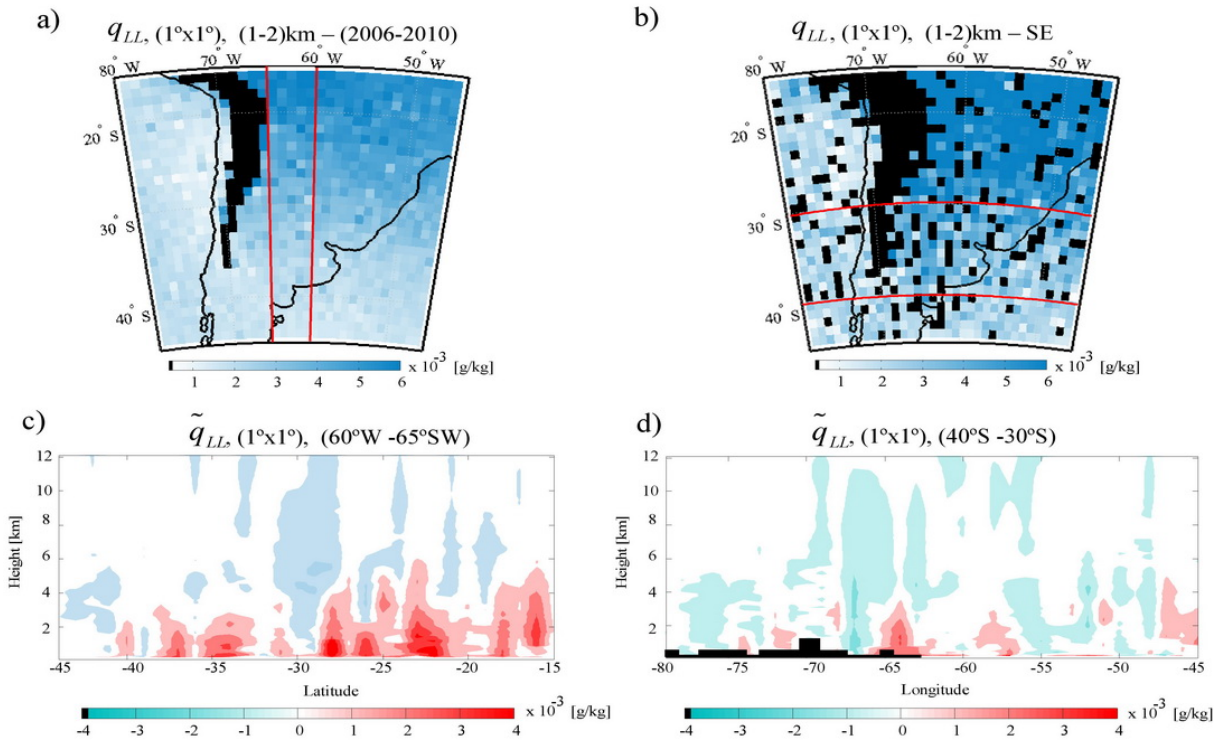

Figure 8. a) q_{LL} 2006-2010 period average and b) q_{LL} averaged in storm events (SE); c) and d) Z-lat (60-65W) and Z-lon (30-40S) slices of q_{LL} anomalies ($\tilde{q}_{LL}$) respectively. The region averaged in these slices are marked in a) and b) with red lines.